

Review

Review of Artificial Nacre for Oil–Water Separation

Apriliana Cahya Khayrani ¹, Nonni Soraya Sambudi ^{2,*}, Hans Wijaya ^{3,*}, Yose Fachmi Buys ⁴, Fitri Ayu Radini ⁵, Norwahyu Jusoh ⁶, Norashikin Ahmad Kamal ^{7,*} and Hazwani Suhaimi ⁸

- ¹ Department of Chemical Engineering, Faculty of Engineering, Universitas Indonesia, Depok 16424, Indonesia
 - ² Department of Chemical Engineering, Faculty of Industrial Technology, Universitas Pertamina, Jakarta 12220, Indonesia
 - ³ Research Center for Applied Microbiology, National Research and Innovation Agency, Jl. Raya Bogor Km. 46, Cibinong 16911, Indonesia
 - ⁴ Department of Mechanical Engineering, Faculty of Industrial Technology, Universitas Pertamina, Jakarta 12220, Indonesia
 - ⁵ Research Center for Polymer Technology, National Research and Innovation Agency, Gedung 460, Kawasan Puspitek Serpong, Muncul, Kec. Setu, Kota Tangerang Selatan 15314, Indonesia
 - ⁶ Department of Chemical Engineering, Universiti Teknologi PETRONAS, Seri Iskandar 32610, Malaysia
 - ⁷ School of Civil Engineering, College of Engineering, Universiti Teknologi MARA (UiTM), Shah Alam 40450, Malaysia
 - ⁸ Faculty of Integrated Technologies, Universiti Brunei Darussalam, Jalan Tungku Link, Gadong BE1410, Brunei
- * Correspondence: nonni.ss@universitaspertamina.ac.id (N.S.S.); hans001@brin.go.id (H.W.); norashikin7349@uitm.edu.my (N.A.K.)

Abstract: Due to their extraordinary prospective uses, particularly in the areas of oil–water separation, underwater superoleophobic materials have gained increasing attention. Thus, artificial nacre has become an attractive candidate for oil–water separation due to its superhydrophilicity and underwater superoleophobicity properties. Synthesized artificial nacre has successfully achieved a high mechanical strength that is close to or even surpasses the mechanical strength of natural nacre. This can be attributed to suitable synthesis methods, the selection of inorganic fillers and polymer matrices, and the enhancement of the mechanical properties through cross-linking, covalent group modification, or mineralization. The utilization of nacre-inspired composite membranes for emerging applications, i.e., is oily wastewater treatment, is highlighted in this review. The membranes show that full separation of oil and water can be achieved, which enables their applications in seawater environments. The self-cleaning mechanism's basic functioning and antifouling tips are also concluded in this review.

Keywords: nacre; layered composite; self-assembly; layer by layer; oil–water separation; antifouling coating



Citation: Khayrani, A.C.; Sambudi, N.S.; Wijaya, H.; Buys, Y.F.; Radini, F.A.; Jusoh, N.; Kamal, N.A.; Suhaimi, H. Review of Artificial Nacre for Oil–Water Separation. *Separations* **2023**, *10*, 205. <https://doi.org/10.3390/separations10030205>

Academic Editors: Daniela Suteu and Carmen Zaharia

Received: 8 February 2023

Revised: 5 March 2023

Accepted: 10 March 2023

Published: 15 March 2023



Copyright: © 2023 by the authors. Licensee MDPI, Basel, Switzerland. This article is an open access article distributed under the terms and conditions of the Creative Commons Attribution (CC BY) license (<https://creativecommons.org/licenses/by/4.0/>).

1. Introduction

Oily wastewater is a type of wastewater with a high oil content, which, in the petroleum industry, can be generated from produced water brought to the surface during oil and gas production. This wastewater can contain many harmful components and usually consists of grease, oil, and other type of hydrocarbons, as well as high levels of metals, salts, and suspended solid elements [1]. The sources of oily wastewater are quite broad, covering offshore drilling, the oil industry, oil refining, oil storage, transportation, and petrochemical industries [2,3]. The estimated global production of crude oil reaches 41 million m³/day, with the production of a barrel of oil also producing three barrels of water [4]. The generation of produced water increases when the oil well ages [5]. The treatment of oily wastewater has been very costly so far, involving several techniques, such

as flotation, coagulation, biological treatment, and advanced oxidation process, including electrochemical catalysis and supercritical water oxidation [6–8]. Any other approaches require a large space, a long processing time, a high cost, and often cannot meet the stringent treatment requirement for discharge or reuse [4,9,10]. Membrane technology has been of great interest due to its potential advantages of simple systems, a short process time and hence small footprint, and high separation efficiency [4]. The membrane selectively separates oil and water through its microporous structure, and could demonstrate high effectiveness of purification [10]. By mimicking the structure of strong natural materials, such as nacre, membranes with advanced, robust, and durable properties can be fabricated.

The organisms in nature have become inspirations in creating advanced materials by mimicking their unique structures. In particular, materials such as shells, lotus leaves, or gecko skin, possessing high mechanical properties, superhydrophobicity, and super adhesiveness, respectively, can be mimicked to fabricate materials with promising features of the mentioned natural materials [11,12]. An excellent example of a strong biological structure is nacre that forms the inside of shells.

Nacre is a material with a hierarchical structure, as can be seen in Figure 1. Its fundamental structure consists of organic and inorganic components, including inorganic aragonite layers within the layers of the polymer matrix [13]. There are two layers with different microstructures observed in shells containing nacre: the calcite layer and an inner aragonite layer [4]. The natural role of nacre itself is to protect the shell from any breakage and damage due to its high mechanical properties [14–18]. Nacre has a tensile strength ranging from 80 to 135 MPa and a Young's modulus from 60 to 70 GPa [19]. Due to its excellent mechanical properties, nacre is of interest to many researchers. The superior mechanical stability of nacre in seashells is related to hard minerals and soft polymers existing in nacre's structure [20]. Nacre owns a brick-and-mortar structure, where soft biopolymers are attached to inorganic hard aragonite layers to form tiles, acting as high-performance adhesives [10,11]. This tough and iridescent biomaterial is made up of 95% aragonite calcium carbonate, which is the rigid part, and glued with 5% of proteins and polysaccharides as biopolymers [20]. The modulus of nacre is far superior compared to cortical bone which is around 10 to 30 GPa [21], and also higher in comparison with peritubular dentin at around 40 to 45 GPa [22].

The structure and properties of natural nacre are excellent; however, it is well known that its production is limited in nature. Hence, artificial nacre is currently being developed with an analysis of the development potential and application prospects of mimicking natural nacre. Many approaches in fabricating artificial nacre have been performed through the self-assembly method, either supported by vacuum filtration or film casting. Additionally, a layer-by-layer synthesis method is also widely used. All fabrication methods aim to synthesize a layered composite mimicking nacre by using various inorganic materials, such as montmorillonite (MMT) [23], graphene oxide (GO) [24], calcium carbonate [25], carbon nanotubes (CNTs) [26], clay [27], zeolite [28], and many more. In order to represent biopolymer, organic materials are utilized to bind the inorganics, such as polyvinyl alcohol (PVA) [29], chitosan [30], sodium alginate (SA) [31], polydopamine [32], polyurethane [33], etc. The synthesized composites exhibit excellent mechanical properties, with a few demonstrating a similar tensile strength to nacre. Additionally, artificial nacre usually exhibits crack deflection from the crack propagation process, which mimics one of the unique properties of nacre. The organic layer acts as viscoelastic glue and connects the mineral bridges to create tablet interlocking during sliding, which contributes to strengthen the nacre [34]. Nacre from the blue mussel, *Mytilus edulis*, is a nonburrowing, epibenthic species that is widespread across the world and frequently appears in large numbers, making it an important potential substrate for both micro- and macrofoulers to settle on. The majority of *M. edulis* shells, nevertheless, are still devoid of fouling organisms [35]. The mechanism of antifouling nacre from *M. edulis* shells can be mimicked for artificial nacre serving as membrane antifouling accessories.

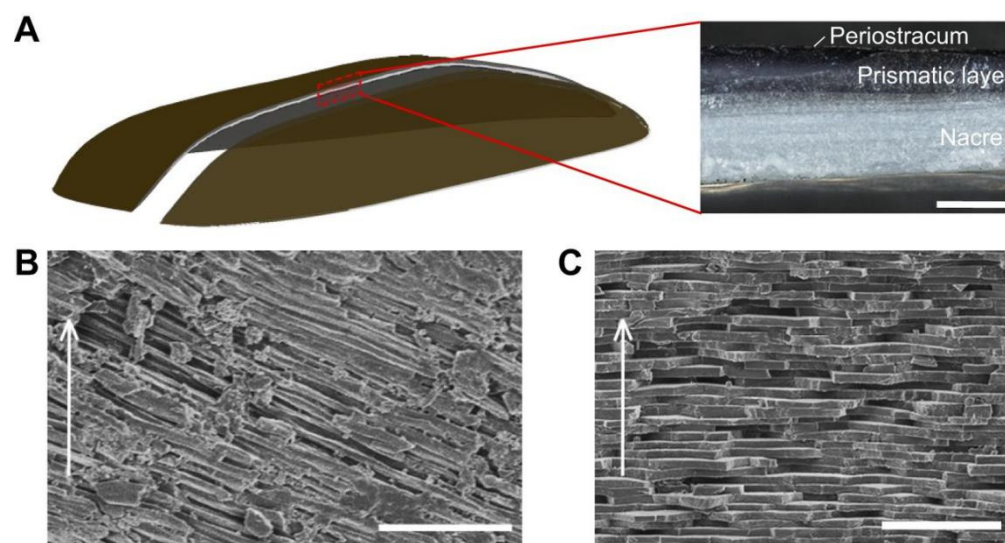


Figure 1. Multiscale structures in *Mytilus edulis* shells. (A) Multilayered structure of the cross-section of the bivalve shell observed under an optical microscope. Three layers are visible from the outside to the inside: the periostracum, the prismatic layer, and the nacre. (B) Scanning electron microscopy (SEM) images of oblique-arranged columnar calcite grains situated in the prismatic layer. (C) SEM image of the brick-and-mortar-like structure of nacre. White arrows in B and C indicate the normal direction of the shell from the inside to the outside. Scale bars: (A), 600 μm ; (B,C), 10 μm . Reproduced from ref. [13] with permission of The Company of Biologists.

In this review, several fabrication methods of nacre-mimetic artificial materials will be discussed, combined with antifouling accessories and the emerging application of the composites for oil–water separation. The production of oily wastewater has been accelerated by the rapid growth of industrialization, in which the untreated oily wastewater can cause fatality to aquatic organisms and even human beings due to the overconsumption of oxygen by the organisms caused by the high content of organic matter [7,10]. Membrane technology has been found to be effective in treating oily wastewater. As a semipermeable membrane between two phases, the water flows through the membrane, and organic matter will be retained on its surface [36]. The layered structure of nacre resembles the structure of the membrane with excellent mechanical strength. Hence, for oily wastewater separation, artificial nacre can be a suitable candidate. To achieve this goal, artificial nacre should possess suitable properties that can retain oil on its surface and allow water to penetrate its layered structure. When the membrane is designed by mimicking nacre, its surface morphology can be controlled to produce a membrane with superhydrophilicity and underwater superoleophobicity equipped with the additional trait of high mechanical properties that can sustain its usability and allow it to be used to separate water and oil [34]. The interests in nacre research are shown to be increasing in Figure 2, started from 2013 until recently, as observed from published papers and issued patents. To the best of our knowledge, a review of nacre for oil–water separation has not been published to date; hence, this review will serve as an interesting discussion on the emerging application of artificial nacre, especially for oily wastewater treatment.

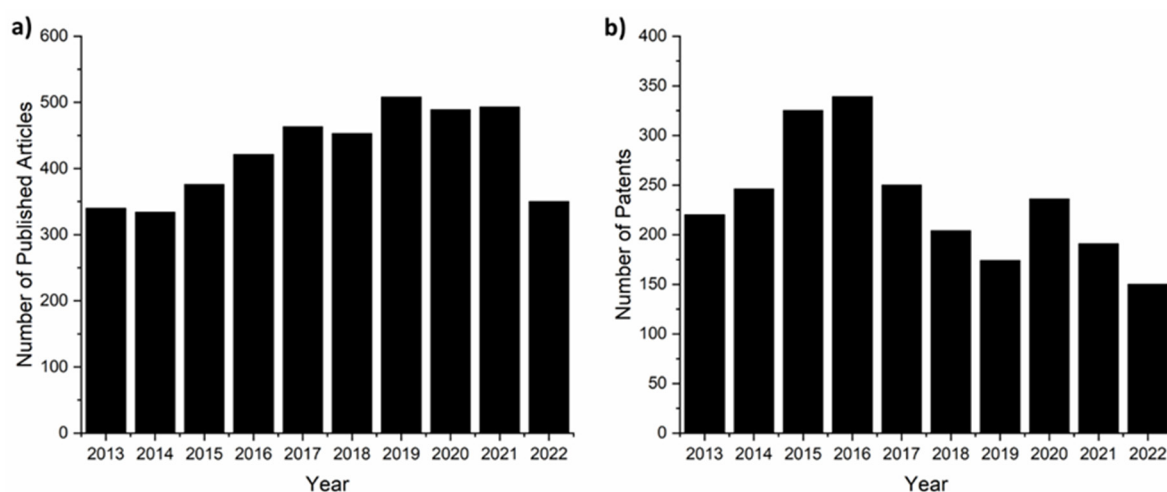


Figure 2. Trend of published (a) papers and (b) patents for artificial nacre. Data extracted from Web of Science for papers and Lens for patents.

2. Fabrication Methods of Nacre-Inspired Materials

2.1. Self-Assembly

An effective way to fabricate a hierarchical system in composites is by using the self-assembly method [37,38]. There are many methods that represent self-assembly, including vacuum-assisted filtration and film casting followed by evaporation. Vacuum-assisted filtration employs a suction pump to create vacuum conditions by using a filtration set-up to produce layered composites. It is one of the most facile techniques, in which the thickness of the composite can be controlled by adjusting the volume of solution [39]. However, this method has been shown to be difficult to fabricate a large-area composite [40]. A previous study attempted to increase the toughness of the composite by synergizing the interface interaction of π - π stacking and hydrogen bonding through sulfonated styrene-ethylene/butylene-styrene (SSEBS) on GO nanosheets, which can improve GO film's tensile strength and toughness from 90 MPa to 158 ± 6 MPa and from 1.53 MJ/m^3 to $15.3 \pm 1.5 \text{ MJ/m}^3$, respectively [41]. The self-assembly of layered composites can also be achieved through film casting. Nanoclay delaminated sodium fluorohectorite (NHT) was used to increase the aspect ratio of nanoclay. By using poly(ethylene oxide), its polymer chain length can be manipulated to bridge nanoclay platelets to achieve a depletion effect to form layered composites with a tensile strength of 99.7 ± 10.3 MPa, and a Young's modulus of 24.3 ± 1.6 GPa [39]. A similar approach was performed by Sung et al. [16] in modifying the surface of MMT through a cation exchange reaction using surfactant (undecyl 10-undecenoyloxy trimethylammonium bromide (UTA)). Functionalization of the MMT surface was performed to incorporate the hydrophobic polymer in layered structures, since MMT is highly hydrophilic and the utilization of a hydrophobic polymer is able to provide a higher mechanical strength, since it will not absorb moisture which can deteriorate the mechanical performance of the composite [27]. The organic acid-induced crystal growth technique is one of the strategies to fabricate a hierarchical structure [42]. In this approach, the organic material is used as a medium to produce inorganic minerals in supersaturated solution [37,42]. The organic part can accelerate or reduce the rate of crystal growth, depending on its molecular weight, functional groups present, concentration, temperature, pH of solution, and other factors [37,42,43]. The absorption of polymers will affect the mineral's growth [44], which was shown in an early study by Sellinger et al. [45]. The study relied on evaporation during the dip-coating technique using homogenous solutions of soluble silicates, a coupling agent, surfactant, organic monomers, and initiators in a water-ethanol mixture to form laminated structures [33]. The evaporation-induced partitioning mechanism was adopted in their study to incorporate alcohol-soluble monomers and initiators into micellar species [45]. The continuous evaporation resulted in the assembly of

micellar species into organized liquid crystalline mesophases, simultaneously organizing both the mineral and organic precursors into laminated structures [34].

Gao et al. demonstrated the scale-up of self-assembly techniques by fabricating a three-dimensional bulk form of artificial nacre via a bottom-up assembly process based on laminating prefabricated two-dimensional nacre-mimetic films (Figure 3) [46]. The fabrication began with a mixture of calcium phosphate platelets and SA inducing facial interaction through Ca^{2+} -SA coordination [46]. The diffusion of Ca^{2+} ions has been shown to induce mineralization which can prevent moisture traps [47]. This mixture underwent evaporation-induced self-assembly, followed by interaction with chitosan through strong electrostatic interaction via the carboxyl groups of SA and the amine groups of chitosan, followed by cross-linking using CaCl_2 which can improve the platelets' orientation degree [46]. This method produced a composite with a tensile strength of around 75 MPa, and a Young's modulus of around 2.1 GPa [46]. However, the ultimate flexural strength at 267 MPa could surpass that of natural *C. plicata* nacre at 172 MPa, but the ultimate stiffness at 18.6 GPa was lower than that of natural *C. plicata* nacre at 48.9 GPa [46]. The biomimetic mineralization approach has been demonstrated to produce high performance bulk materials [48].

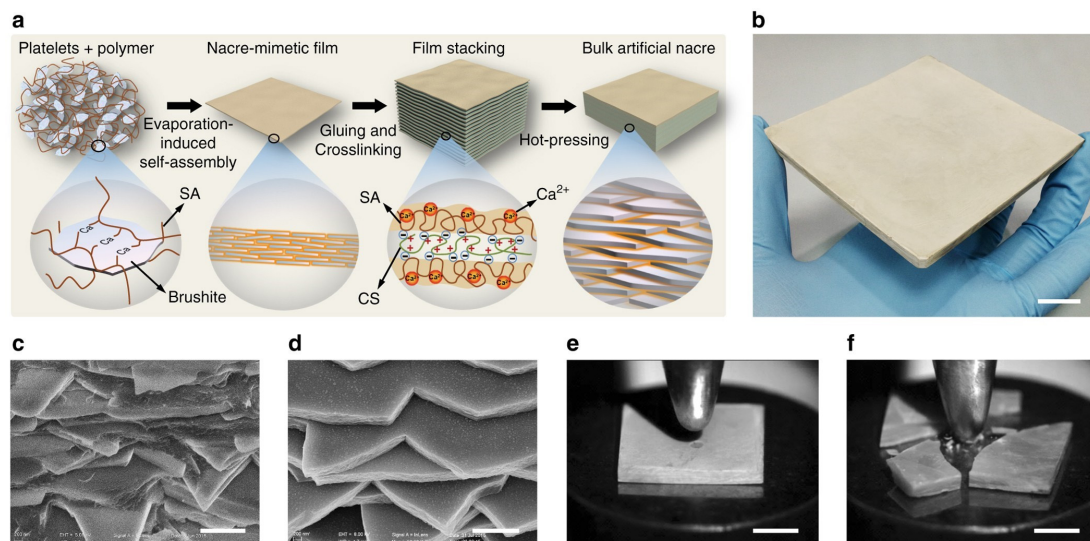


Figure 3. Fabrication and characterization of bulk artificial nacre. (a) Schematic illustration of the bottom-up assembly process of bulk artificial nacre. (b) Large as-fabricated bulk artificial nacre. Scale bar, 2 cm. Cross-section of the (c) artificial nacre and (d) natural *Cristaria plicata* nacre showing a similar fractured layered microstructure. Scale bars, 1 μm . (e) Artificial nacre and (f) *Cristaria plicata* nacre under the same strength of impact, illustrating the higher impact resistance of the artificial nacre. Scale bars, 5 mm. Reproduced from ref. [46] with permission from Springer Nature.

The synthesis of the transparent layered composite mimicking nacre was successfully performed using synthetic nanoclay and PVA. The transparency was formed at a low aspect ratio, where irregularities and grain boundaries must be prevented to reduce light scattering within the film. At the same time, the surface must contain a minimum roughness to avoid surface scattering [49]. However, this effect became less prominent in high aspect ratios when the composite turned opaque [49]. The advancement of layered composite synthesis has also been directed towards smart materials. Du et al. [50] controlled the polymer chain dynamics to permanently program the composite's shape through plasticity and temporarily through shape memory effects. Hence, the self-healing and programming capabilities became interesting traits of smart nacre [50]. The densified alumina platelets were aligned to three-dimensional porous structures via bidirectional freezing [50]. In order to achieve smart nacre, infiltration of a Diels–Alder network polymer was performed into the densified alumina platelets in liquid precursor form, followed by thermal curing [50].

The dynamic of the Diels–Alder polymer network plays an important role, since reversible Diels–Alder chemistry allows the healing of internal damage and polymer–filler interface by reforming the network structure, hence providing the composite with a self-healing property [51]. This delicate material design enables the property to be extended to shape programming, where the temporary shape programming can be applied upon cooling, and permanent shape programming can be applied via plasticity [50].

2.2. Layer-by-Layer

A layer-by-layer method is a strategy to produce functional multilayer thin films and has been adopted to fabricate various materials. Ultrathin films with multilayered structures are produced by sequential adsorption of a cationic polyelectrolyte and anionic mineral platelets via layer-by-layer methods [29,52]. One of the most widely used techniques to fabricate layered materials is by using spin coating through layer-by-layer bottom-up colloidal assembly, as can be seen in Figure 4. By using this method, the layered material can be peeled after synthesis with high flexibility and sufficient ductility [29]. The advantage of this method is that the thickness of the inorganic–organic layers can be tuned by altering the rotation speed during the spin coating process [39]. The layer-by-layer method successfully fabricates artificial nacre which mimicked not only nacre’s mechanical properties, but also its iridescence properties [51]. A study by Finnemore et al. [51] proposed essential steps to fabricate essential nacre using amorphous calcium carbonate (ACC), beginning from (1) the stabilization of ACC in solution, followed by (2) specific aggregation and continuous film formation on organic surfaces, (3) the deposition of a porous and suitably functionalized thin organic film on the formed mineral layers, (4) the crystallization of ACC to form aragonite or calcite, and then (5) the cyclical iteration of steps 1 to 4. This study also presented an important factor governing the successful formation of the artificial nacre, which is that mineral continuity across the porous organic layers should be available to form a microstructure of the nacre [51]. Additionally, the porous organic interlayer is substantial since it will allow the formation of bridges between mineral films that grow and propagate across the organic layers, contributing to the mechanical stability of the composite [51]. Therefore, a good control of layer periodicity through multilayer stacks resulted in nacre’s iridescence [51]. Farhadi-Khouzani et al. [53] also successfully fabricated an iridescent layer composite using CaCO_3 and nanocellulose via sequential infiltration of polymer-stabilized CaCO_3 precursors into layers of pre-deposited nanocellulose films. The functionalization of nanocellulose was performed using hydroxyl groups (Na-OH), which provide good wettability for CaCO_3 mineralization, which was optimized by adjusting the ratio of the concentrations of calcium chloride and poly(aspartic acid) [53]. The functionalization of nanocellulose was also performed using carboxyl functional groups (Na-COOH), which cannot be wetted in the absence of Mg^{2+} and unmineralized [53]. The layered of unmineralized nanocellulose was alternated with mineralized layered of nanocellulose repeatedly until the iridescent composite was formed [53]. This study is in agreement with a previous study by Finnemore et al. [51], in which the existence of multiple uniform layers produced the interference composite [53]. The layered composite can be fabricated to produce 90 layers resulting in a hardness of 222.5 ± 23.6 MPa and a Young’s modulus of 14.4 ± 1.7 GPa [53]. Table 1 provides the comparison of the synthesized composites’ mechanical properties from various synthesis methods.

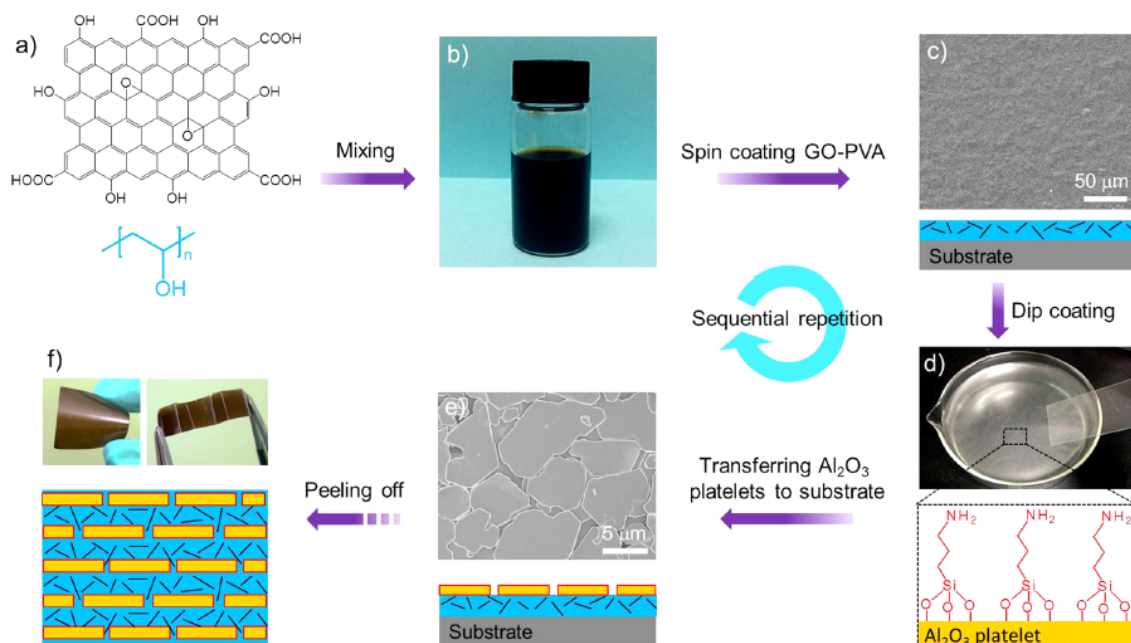


Figure 4. Layer-by-layer bottom-up assembly of multilayered Al₂O₃/GO–PVA artificial nacre. (a) GO and PVA. (b) Mixing of PVA and GO nanosheets. (c) Spin coating one layer of GO–PVA onto a glass substrate. (d) Assembling silane-modified Al₂O₃ microplatelets into a monolayer at the air–water interface. (e) Transferring the assembled Al₂O₃ monolayer onto the GO–PVA layer. (f) The obtained flexible, foldable artificial nacre after sequential repetition. Reproduced from ref. [29] with permission of the American Chemical Society.

Table 1. List of mechanical properties of layered composite mimicking nacre.

Synthesis Method	Materials	Mechanical Properties			Reference
		Yield Strength (MPa)	Hardness (MJ/m ³)	Young’s Modulus (GPa)	
Layer-by-layer	Gold nanoparticle/PVA	122	-	8.5	[54]
Layer-by-layer	Al ₂ O ₃ /GO/PVA	143 ± 13	9.2 ± 2.7		[29]
Cross-linking of alginate with Ca ions	MMT/CaCl ₂	280	7.2		[31]
Evaporation-induced self-assembly	Clay platelet/nanofibrillar cellulose/PVA	80–135	1.8		[55]
Spin-coating	Zeolite/CdSe-zeolite/PVA	70			[28]
Vacuum-assisted self-assembly	Noncovalent functionalized boron nitride nanosheets/PVA	125.2	2.37		[56]
Continuous wet-spinning assembly	PVA-coated graphene	161			[57]
Film casting	Reduced GO (rGO)/PVA/single-walled carbon nanotubes (SWCNT)	62.8		0.55	[58]
Hot press and curing	Ag-boron nitrite/epoxy	80.3	0.35	23.4	[59]
Combination of ball-milling and hot-rolling	Graphite nanosheets/Cu	660		170	[60]
Lanthanide ion coordination	Sodium alginate biopolymers/lanthanide ions (Nd ³⁺ , Gd ³⁺ , Ce ³⁺ , and Yb ³⁺)	124.2 ± 5.2	8.2 ± 0.4	5.2 ± 0.2	[61]
Vacuum-assisted self-assembly	GO/PVA	360.7		42.2	[62]
Waterborne dispersion casting method	Nanoclay/polyethylene oxide (PEO)	99.7 ± 10.3		24.3 ± 1.6	[39]

Table 1. *Cont.*

Synthesis Method	Materials	Mechanical Properties			Reference
		Yield Strength (MPa)	Hardness (MJ/m ³)	Young's Modulus (GPa)	
Vacuum-assisted self-assembly with ultrafiltration	MMT/aramid nanofiber	126.5			[63]
Solution-casting and in situ chemical reduction	Graphene/polybenzimidazole (PBI)	77.7		6.33	[64]
Bottom-up assembly process based on laminating prefabricated two-dimensional nacre-mimetic films	Brushite (CaHPO ₄ ·2H ₂ O) platelets/SA	267			[46]
Film casting and cured	Borate cross-linked galactomannan/GO	135.54			[65]
Film casting and cured	MMT/poly(3-mercaptopropyl)methylsiloxane (PMMS)	64–110		5–12	[27]
Vacuum-assisted self-assembly	Boron nitride nanosheets (BNNs) and graphene oxide (GO)	16.3		6.5	[66]
Vacuum-assisted self-assembly	GO/carboxyl functionalized SWCNT/konjac glucomannan	311.4 ± 9.2	11.1 ± 0.5		[26]
Stirring and ultrasonic treatment	GO-CNT/thermoplastic polyurethane	209.8	5		[67]
Evaporation-based self-assembly	MMT/chitosan/genipin/NaOH	226	5.1		[23]
Filtration and cross-linking	GO/p-diaminophenyl	142.9 ± 6.4		4.7 ± 0.36	[68]
Filtration and vacuum drying	Polydopamine-capped graphene oxide (PDG)/2-ureido-4[1H]-pyrimidinone hexamethylene isocyanate (UPy-NCO)	325.6 ± 17.8	11.1		[69]
Vacuum-assisted self-assembly	Boron nitride nanosheets/gelatin	148.7		31	[70]
Modified bidirectional freezing technique	GO/PVA	150.9	8.5		[71]
LBL assembly and the VAF method	Polyurethane/aramid nanofibers	98.02		5.275	[33]
Wet-spinning	MMT nanoplatelets/graphene	88–270			[72]
Multi-step powder metallurgy route and industrial extrusion process followed by laser shock peening	Graphene/aluminum alloy	343		79.8	[73]
Film casting	Mg-amorphous calcium carbonate (ACC)/chitosan	121.67		31.96	[30]
Vacuum-assisted self-assembly	1D 2,2,6,6-tetramethyl-1-piperidinyloxy (TEMPO)-oxidized cellulose nanofibers/MXene	128.13		7	[74]
Vacuum-assisted self-assembly	PVA/hydroxylfunctionalized black phosphorus (BP-OH)/GO	74.3 ± 3.5			[75]
Vacuum-assisted resin infusion molding process	MMT-MWCNT/epoxy	750		36	[76]

3. Antifouling Coating for Artificial Nacre Inspired by Natural Nacre

The reduction in surface fouling in nacre *M. edulis* shell cannot be explained by the active cleaning of the shell by the mussel's foot, as this cleaning mechanism is only effective for individuals shorter than 3 cm in length [77]. This explains other strategies for antifouling in nacre *M. edulis* shell that served as accessories that can be used chemically and enzymatically.

3.1. Chemical Antifouling Accessories

The antifouling capacity by crude extracts of *M. edulis* periostracum against representatives of significant fouling groups, such as bacteria, diatoms, and barnacles, was effectively investigated in the study by Bers [35]. Bers' work used solvents of increasing polarity, where six rough extracts of the periostracum of whole shells were synthesized. Lab-based bioassays were performed, and these extracts were evaluated for their ability to inhibit common fouling species. The diethyl ether fraction strongly inhibited the *Balanus amphitrite* cyprid attachment, as well as the attachment of the marine bacteria *Cobetia marina* and

Marinobacter hydrocarbonoclasticus at the specified dosages. The dichloromethane fraction greatly decreased the diatom attachment of *Amphora coffeaeformis*, but the ethyl acetate and diethyl ether fractions both inhibited the development of the benthic diatom [35].

3.2. Enzymatic Antifouling Accessories

Enzymatic antifouling can be explained by the studies of the live *M. edulis* which reveal that they actively clean their shells and that the foot is anatomically suited to the cleaning process. The mucous glands on the dorsal side of the foot make it easier for the foot to slide over the shell when cleaning, and they may also produce a mucoprotein that acts as a protective agent on the shell while cleaning [77]. This mucoprotein in *M. edulis* digestive systems contains several enzymes, such as amylase [78,79], lysozyme [80], protease, lipase [78], etc.

By mimicking this antifouling via an enzymatic process in the nacre surface, the modification of the surface of membranes can be undertaken. Surface modification of membranes has emerged as a major technique for their functionalization [81]. One method of membrane modification is to decrease fouling, which may be accomplished via the immobilization of α -amylase nanoparticles as an antifouling agent for carbohydrates. The immobilized α -amylase is combined with lipase to provide self-cleaning properties for carbohydrates, lipids, and proteins on polyvinylidene fluoride (PVDF) membranes [82]. In the hydrolysis process of microbial macromolecules in bioreactors, immobilized amylase on microfiltration membranes can reduce cake density and resistance [83]. Other modifications, such as the use of polyethersulfone membrane with α -amylase, were proved to result in a higher stability, a higher activity, and successful membrane regeneration [84].

The combination of α -amylase and lysozyme proves to not only improve membrane surface anti-biofouling properties but also remove bacterial pathogen contamination [85]. A combination between protease and α -amylase immobilized on electrospun nanofibrous materials also can degrade proteins and starch in solution [86]. Therefore, it is important that the coating present on natural nacre is applied to artificial nacre in order to exhibit self-cleaning properties. The initial part of the process of self-cleaning membranes (Figure 5) is the immobilization of digesting enzymes on the membrane surface, which brings both enzymes and fouling compounds adsorbed on the surface into contact. Finally, by activating the digestive enzymes via modifying the surrounding circumstances, the fouling layer that accumulates during filtering may then be eliminated enzymatically via hydrolysis.

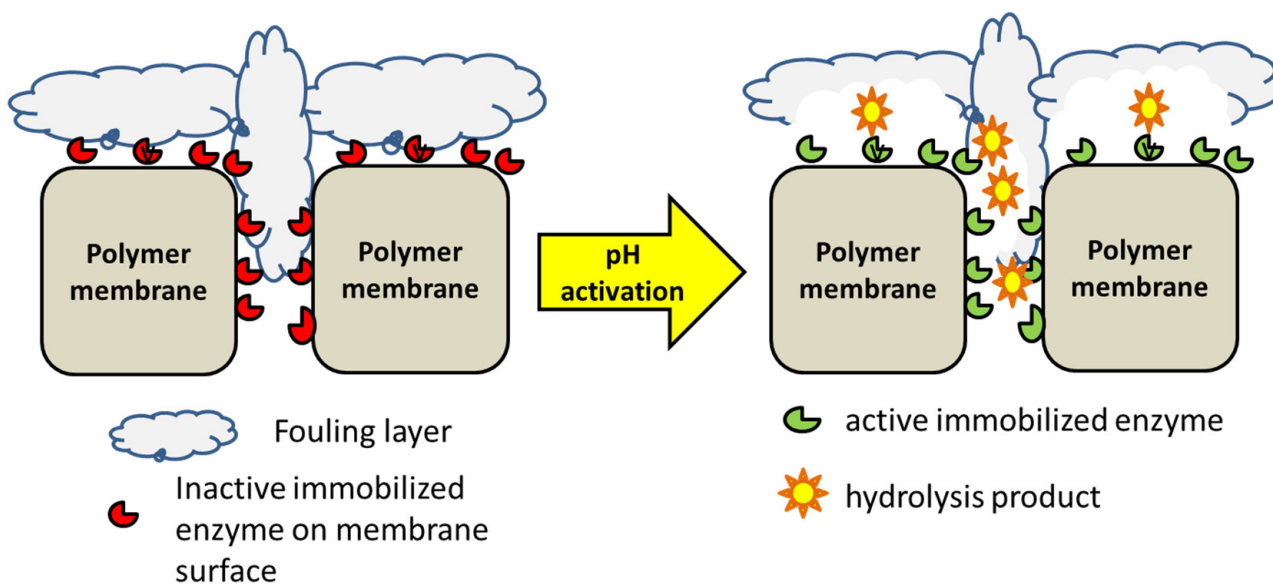


Figure 5. Schematic mechanism of self-cleaning membranes. By altering the pH of the buffer, digestive enzymes immobilized on the membrane surface become active and break down the substrates that cause fouling. Reproduced from ref. [82] with permission of Elsevier.

Other combinations of polyethersulfone membranes with α -amylase integrated in chitosan-based polymeric micelles increase coating durability, which is attributed to the surface-active characteristics of chitosan derivatives and electrostatic interaction [87,88]. The use of chitosan combined with catechol by using a one-step oxidant-induced ultrafast co-deposition on a porous PVDF substrate was presented as a simple green method for the production of an underwater superoleophobic microfiltration membrane. This technique for oil–water separation showed outstanding anti-oil fouling and reusability. Its strong performance was caused by the hydrophilic coating's induction of the creation of an interfacial hydration barrier within the porous structure. The mechanism attachment of oil droplets to the membrane surface can be effectively avoided by this hydration layer. However, due to the membrane's attraction to water, water may quickly pass through the membrane [88]. The pure PVDF membrane, on the other hand, had a great attraction to oil droplets, which led to severe pore clogging and surface fouling, increasing the filtering resistance [88].

Beside these approaches, the coating of membranes with organic or inorganic constituents has proven to be effective to prevent fouling, by increasing the surface roughness of the material. In a previous study by Wang et.al., when coating mesh with a combination of chitosan/kaolin/ CaCO_3 , it was found that irregular micro/nanoparticles form on the surface of the mesh, which reduce the fouling of the membrane significantly [89]. A hierarchical micro/nanoscale structure was also presented in the study of Dai et.al., which was shown to improve the surface hydrophilicity and reduce fouling [24]. However, if fouling still occurs due to long operation time and build-up of oil, regeneration can take place through hydraulic and catalytic cleaning. Hydraulic cleaning can be undertaken through a backwashing membrane at a pressure of around 0.75 bar for several minutes [90], while catalytic cleaning can be performed by using peroxydisulfate, by generating active species that have strong oxidation ability [90]. These active species can penetrate the pores during the cleaning process and degrade the build-up through physicochemical cleaning [90].

4. Oil–Water Separation

4.1. Hydrophilicity and Oleophobicity of Membranes

The oily wastewater can be generated from various sources, such as mining, petrochemical, metal/steel industries, or even oil spills [91]. The oily wastewater discharged from the oil and gas industry usually originated from produced water. The typical oil and grease content covers hydrocarbons, solid particles, heavy metals, and other toxic materials [92]. The oil content to be safely discharged to seawater is usually in the range of 10–15 mg/L, since higher concentration can destroy ecosystems, crop production, and the death of marine life [62]. Besides the produced water, oil spill incidents have caused a loss of oil resources and huge costs in cleaning tons of oils.

Membranes have been recognized as one of the technologies that can effectively remove oil from the aquatic environment due to their cost-effectiveness and reusability [61]. To effectively treat oily wastewater, the membrane should develop superhydrophilicity and underwater superoleophobicity properties [25,63,64]. Until now, only a few studies were published in applying artificial nacre or material inspired from mussels to treat oily wastewater (Figure 6) [93–96]. However, the biomimetic concept offers many advantageous properties to membrane applications, in which oil–water separation can serve as one of the emerging applications. The superhydrophilicity and superoleophobicity properties, as special wettability traits in the membrane, can be induced through coatings, surface oxidation, and modification of the surface, which could govern the contact interfaces of solid, water, and oil phases [97]. The superhydrophilic–underwater superoleophobic membrane repels oil while allowing water to pass through the membrane, minimizing the fouling of the membrane and developing a self-cleaning material [69]. In this type of membrane, the oil repellence is due to the liquid barrier created by water attached to the membrane surface; hence, pre-wetting of the membrane is an important step to

do [68]. However, Cao et al. [66] used a different approach by creating a hydrophobic and superoleophilic mussel-inspired layered material and were able to perform oil–water separation. Polydopamine was conjugated with n-dodecyl mercaptan through a Michael addition reaction, which was proven by the detection of sulfur element [66].

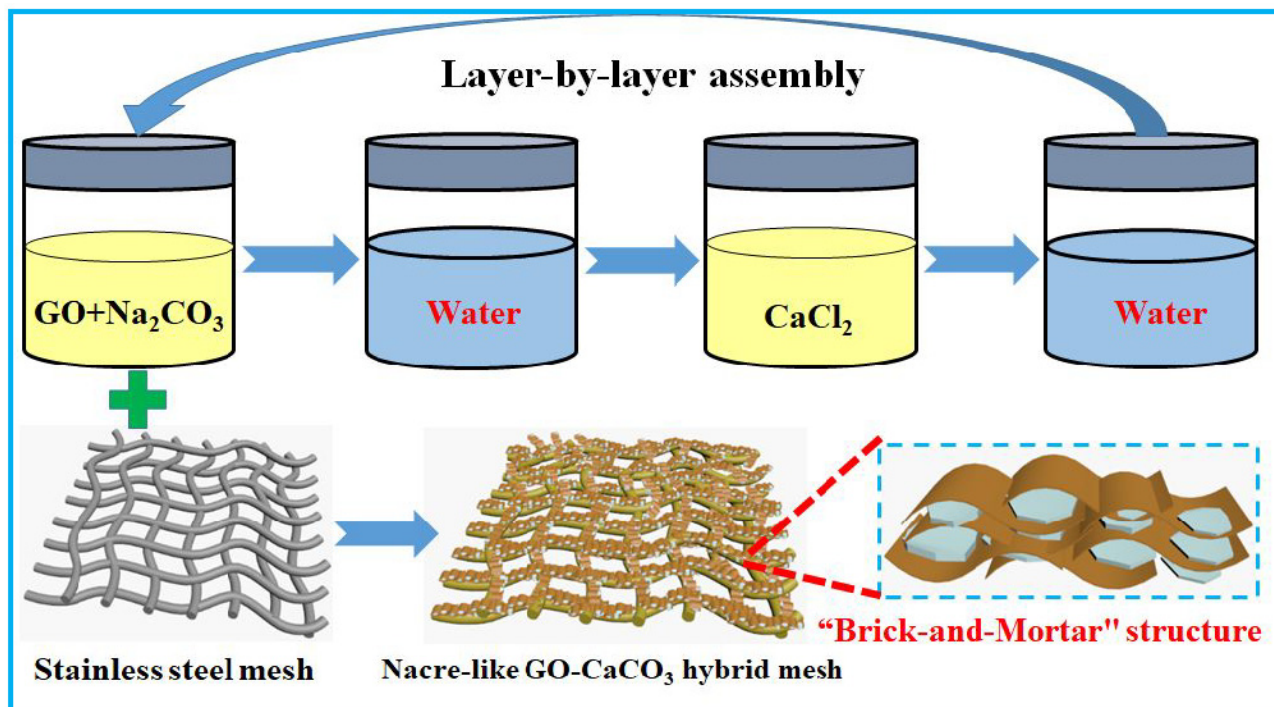


Figure 6. Schematic description of the fabrication of the nacre-like GO-CaCO₃ hybrid mesh for oil–water separation. Reproduced from ref. [24] with permission of the American Chemical Society.

The microstructure on the membrane surface might increase its roughness, which amplified its hydrophilicity, and could be achieved by incorporating inorganic fillers in the membrane matrix [68]. Dai et al. [13] used a GO-CaCO₃/stainless steel mesh to produce superhydrophilic–underwater superoleophobic membranes, in which GO regulates the CaCO₃ crystallization to form a brick-mortar structure (Figure 5). The formation of a thin and wrinkled corrugation surface mimicking the lotus leaf was observed, which is CaCO₃ crystals wrapped by GO nanosheets [13]. The underwater oil contact angle (UOCA) and water contact angle were around 155° and below 3°, respectively, showing underwater superoleophobicity and superhydrophilicity characteristics [13]. The separation efficiency could reach more than 99%, with self-gravity as the only driving force [24]. The membrane is also reusable, with a decrease in performance of only 0.17% after 30 cycles of filtration [24]. In order to observe the stability of the membrane in a marine environment, it was immersed in hyper-saline solutions for several days, and after immersion, the UOCA was still maintained at 154.7° [24].

A previous study used MMT/poly(diallyldimethylammonium chloride) (PDDA) to synthesize a layered material with low surface adhesion force towards oil [98]. The sand abrasion test using sand grains with a diameter of 150–300 μm, which impinged the membrane’s surface from a height of 15 cm, showed good membrane resistance since it retained its underwater superoleophobicity [64]. Additionally, exposure of the membrane in artificial seawater after several days demonstrated the membrane’s durability, where the oil-repellant property could be maintained with UOCAs varying from 158.3° to 163.6° toward n-decane [98].

A study by Li et al. [67] used seeded mineralization of the CaCO₃ technique to form a prismatic-type mineral, which can be found in mollusk shell, and the micro/nanotexture of overlayers on chitosan film. Chitosan as a base was prepared in thin-film form using

spin coating, followed by the diffusion of CO₂ in the presence of poly(acrylic acid sodium salt) (PAA) to form a seed layer [67]. The overgrowth of calcitic prismatic layers was performed using CaCl₂ solutions with poly-L-γ-glutamic acid sodium salt (PGlu) [96]. By varying the concentration of organic constituents, such as PGlu, the morphology of the calcitic overlayer can be controlled, which affects the surface contact angle [67]. The repeated seeded mineralization process forms a hierarchical structure, which mimicked the mollusk shell [96]. The formation of a continuous overlayer can be ascribed to pre-adsorption of polymer additives on seed layers; hence, the polymer additive, in this case chitosan, affects the hierarchical structure of the composite [96]. The utilization of a columnar-shaped inorganic to produce the underwater superoleophobic membrane was also performed by Guo et al. [93]. The columnar nacre was prepared by pouring the solution of MMT/hydroxyethyl cellulose (HEC) in hexagonal silicon honeycomb as a template, which contributes to the underwater low adhesion and superoleophobicity of the composite [93]. The cross-linking of composites was proven to be effective. It contributes to improving the tensile strength of the composite to around 129.3 MPa, which is comparable to natural columnar nacre ranging from 80 to 135 MPa [63]. The stability of the columnar structure on the surface of membranes was beneficial to tolerate the abrasion of sand grains without visible loss the in oil-repellent capability [93]. The membrane was also tested by submerging it in a complex seawater environment for several days, and the UOCA only slightly changed to $159.2 \pm 4.2^\circ$ – $168.2 \pm 4.8^\circ$ from $168.3 \pm 2.8^\circ$ [93].

A study by Li et al. [65], inspired by mussels and lotus leaves, used a polyurethane (PU) sponge which was covalently modified with polydopamine, silver nanoparticles, and dodecyl mercaptan to produce a superhydrophobic/superoleophilic material. The superhydrophobic property of the sponges was synthesized by modifying the sponge with dodecyl mercaptan in ethanol to decrease the surface tension [94]. The modification of sponges by polydopamine and silver caused the roughness to increase on its surface, which repels water and can only be wetted by oil [94].

4.2. Performance of Membranes

The performance of membranes for oil–water separation is given in Table 2. The materials show satisfying performance in oil and water separations, with more than 90% of separation observed, generally through gravity-driven oil–water separation. Li et al. [64] tested the sponge's performance consisting of PU-polydopamine/Ag/dodecyl mercaptan for oil absorption with a complete separation of n-octane/water [64]. The reusability of the sponges was confirmed after five absorption/desorption cycles, in which the oil absorption capacity of materials was still comparable to freshly coated samples [65]. The filtration process using sponge was also tested for a mixture of n-octane and methylene blue (5 ppm), which can be separated with oil penetrated through the sponge quickly, and methylene blue can be collected on the surface [65]. The sponge shows excellent environmental and chemical stability against acid, salt, and alkali solutions, UV irradiation at 200 to 400 nm, and very high and low temperatures [94]. The layered membrane of polydopamine-n-dodecyl mercaptan fabricated on top of a stainless-steel mesh showed stable performance even after 30 rounds of filtration; the separation efficiency could be maintained above 99.5% [65]. The average intrusion pressure of membranes was measured at 2.18 ± 0.08 kPa, which is an important factor in preventing water flow through membranes [65].

Table 2. Comparison of performance of nacre-inspired materials for oil–water separation.

Synthesis Method	Materials	Mechanical Properties		Performance	Reference
		Tensile Strength (MPa)	Young's Modulus (GPa)		
Vacuum-assisted self-assembly	Clay/PNIPAM	0.95	0.0147	Act as oil repellent and could separate 99.9% hexane/water and crude oil/water completely. UOCA of 159°.	[34]
The mixture was shaken at 50 °C to form sponges	PU-polydopamine/Ag/dodecyl mercaptan	0.218 ± 0.021		Complete separation of n-octane/water. Could absorb various types of organic solutions with absorption capacity ranges from 18–43 g/g. The highest absorption capacity was for tetrachloromethane, while the lowest is for crude oil. Water contact angle of 155° and UOCA 0°, hence a superhydrophobic and superoleophilic material.	[94]
Layer-by-layer self-assembly by dipping and washing	GO/CaCO ₃		25.4 ± 2.6	Separation of solutions containing cyclohexane, toluene, diesel, hexane, and petroleum ether, with water flux reaches 179,640 Lm ⁻² h ⁻¹ for cyclohexane and 120,000 Lm ⁻² h ⁻¹ for diesel. UOCA of 155°.	[24]
Spin/dip coating-seed mineralization	Chitosan/CaCO ₃ -Pglu		32.1 ± 9.0	Separation of solutions containing cyclohexane, soybean oil, toluene, silicon oil, and engine oil, with oil concentrations after separation below 4 ppm for soybean oil and below 2 ppm for the rest. UOCA of 145.3 ± 1.6°.	[96]
Film casting-evaporation	MMT/HEC	129.3 ± 6.7	6.3 ± 0.36	UOCA of various oils is higher than 156.8° and adhesive force of less than 3.5 μN.	[93]
Dip coating-wash repeatedly	MMT/PDDA		9.4 ± 2.4	UOCA of various oils are higher than 160° and adhesive force of less than 4.7 ± 2.7 μN.	[98]
Dip coating	GO			Separation efficiency of around 98 and 90% for light oil/water and heavy oil/water, respectively. UOCA above 150°.	[99]
Michael addition reaction	Polydopamine-n-dodecyl mercaptan/stainless steel mesh			Separation efficiency of 99.95% for hexane/water mixture, above 99.7% for petroleum ether and gasoline mixtures, and 98.12 ± 0.31% for diesel/water mixture. Water contact angle of 144° and UOCA 0°, hence a superhydrophobic and superoleophilic material.	[95]
Interfacial assembly and cross-linking	GO/sodium alginate/CaCl ₂		35.8 ± 4.9	Separation efficiency of 99.6% for cyclohexane-water mixture with UOCA of 154 ± 1°.	[100]
Electrospinning	Silica/nafion			Complete separation of carbon tetrachloride and benzene from water. Contact angle of 130°.	[101]
Solution casting	PAA/polyvinylidene fluoride (PVDF)-graphene nanosheet	92.10 ± 10.01	21.28 ± 2.86	UOCA of more than 150°. High mechanical stability after 5 h immersion in seawater (tensile strength and Young's modulus changed to 84.7 ± 9.07 MPa and 12.96 ± 2.48 GPa, respectively).	[102]
Vacuum-assisted self-assembly	Polyethyleneimine (PEI)-CNT	86	4.043	UOAC of around 169.1°, 160.8°, 173.4°, 162.9°, and 168.9° for hexadecane, heptane, soybean oil, pump oil, and silicone oil, respectively. Oil–water separation performance: flux reached 1427 Lm ⁻² h ⁻¹ and flux recovery ratio of 81.7%.	[103]
Facile and green layer-by-layer (LbL) assembly	Chitosan/carboxymethyl cellulose@CaCO ₃			UOAC of 152°, 154°, 151.5°, 150.5°, and 151° for methanol, ethanol, chloroform, toluene, and n-hexane, respectively. Oil–water separation performance: flux reached 7532 Lm ⁻² h ⁻¹ and efficiency can be maintained at 97.8% after 64 times usage.	[104]
Layer-by-layer self-assembly by dipping and rinsing	Chitosan/kaolin@CaCO ₃			UOAC of > 152.5° for gasoline and diesel. Oil–water separation performance: the flux reached 48,520 Lm ⁻² h ⁻¹ and efficiency can be maintained at 97.7% after 64 times usage. Separation efficiency of >98.4% for petroleum ether, kerosene, gasoline, diesel, xylene, and cyclohexane.	[89]

Wang et al. [70] fabricated an alginate/GO nacre mesh and tested it for the separation of various types of oils, such as toluene, cyclohexane, diesel, dichloromethane, and 1,2-dichloroethane, with more than 99% separation, and the highest water flux was found for the cyclohexane–water mixture at $119,426 \text{ Lm}^{-2}\text{h}^{-1}$. The chemical stability of the nacre mesh was performed at pH range from 3 to 9, and the contact angle only slightly decreased at pH 2 from 154° to 153° , and at pH 10–12 from 154° to 152° . Therefore, the mesh showed resistance towards acids and alkalis, which is promising for its application in complex oily water systems.

4.3. Mechanical Properties

The mechanical stability of artificial nacre for oil–water separation is strongly influenced by its building blocks. For oil–water separation, MMT exhibited very high mechanical properties at around $129.3 \pm 6.7 \text{ MPa}$ and $6.3 \pm 0.36 \text{ GPa}$ for tensile strength and the Young's modulus, respectively [93]. The orientation of MMT and cross-linking by HEC are the main factors that contribute to the superior mechanical properties. The MMT platelets have a high weight fraction and are oriented mainly along the plane direction, and chemical cross-linking through glutaraldehyde can strengthen the columnar nacre-like structure [63]. Additionally, the stiffness of the film's surface microstructure is ensured by the perpendicular orientation of MMT platelets in the column wall to the film plane [63].

The phenomenon of high nanofiller loading has emerged to provide the synthesized materials with excellent properties, with one of them being excellent mechanical properties. The unidirectional orientation of platelets might contribute to a high tensile strength, while the strong interaction between the filler and polymer might contribute to the high modulus of composites [76]. The ductility of the material can be achieved through synergetic effects of covalent and noncovalent bonding, such as hydrogen bonding, π – π interaction, etc. [105,106]. The fabrication method, such as the layer-by-layer method, self-assembly, sol–gel techniques, etc., also influences the resulting mechanical properties of the materials. These employed techniques could control a high-filler content through homogeneous dispersion, as well as the interaction force between fillers and polymers [106]. A study by Rashid et al. [78] emphasizes strong electrostatic and hydrogen bonding between PEI and MMT. It enables the composite film to exhibit a modulus of $\sim 65 \text{ GPa}$ through a layer-by-layer method of fabrication.

5. Interaction between Inorganic and Organic Constituents in the Membrane

The emulation of the mechanical strength of nacre is an important factor in the fabrication of artificial nacre. Various methods have been employed to facilitate the formation of bonds among the inorganic and organic components that are expected to improve the mechanical properties and stability of materials (Figure 7). A study by Song et al. [28] used SSEBS in intercalation through GO nanosheets' layers. The interaction between the poly(styrene) part in SSEBS and GO was found through π – π stacking, and hydrogen bonding was formed between sulfoacid groups of SSEBS and oxygen-containing groups on the surface of GO [28]. The interlocking of GO nanosheets through these bonds allows the mutual slippage, which helps dissipate fracture energy and enhances tensile strength [28].

The cross-linking of inorganic and organic components has also been shown to effectively improve the artificial nacre's mechanical properties. One of the cross-linking strategies is through the dipping of sodium alginate-GO in a CaCl_2 solution, which then induces the formation of nanoscale Ca-alginate hydrogel particles between the interlayer of GO nanosheets, to eventually facilitate the mechanical interlocking alongside the formed hydrogen bonds between sodium alginate and GO [70]. Sung et al. [16] applied another strategy using UV irradiation to facilitate an in situ thiol-ene click reaction between the siloxane-based polymer and clay platelets. The thiol-ene click reaction induced the formation of gel-like deposits, which then form a cross-linked layered structure when dried [16]. The in situ reaction between the thiol groups of polymers and ethenyl groups of clay platelets resulted in aggregation due to the high aspect ratio of clay; hence, the gel-like

deposit could be formed [16]. Wang et al. [41] showed the importance of the cross-linker in the layered composite, which could replace the weak van der Waals forces with chemical interactions. High valence Al^{3+} ions were used to enhance the interlayer bonding strength of the spin coating, indicated by the bonding of Al^{3+} with oxygen-containing functional groups on GO nanosheets, which decreased the mixed dispersion's zeta potential value [75].

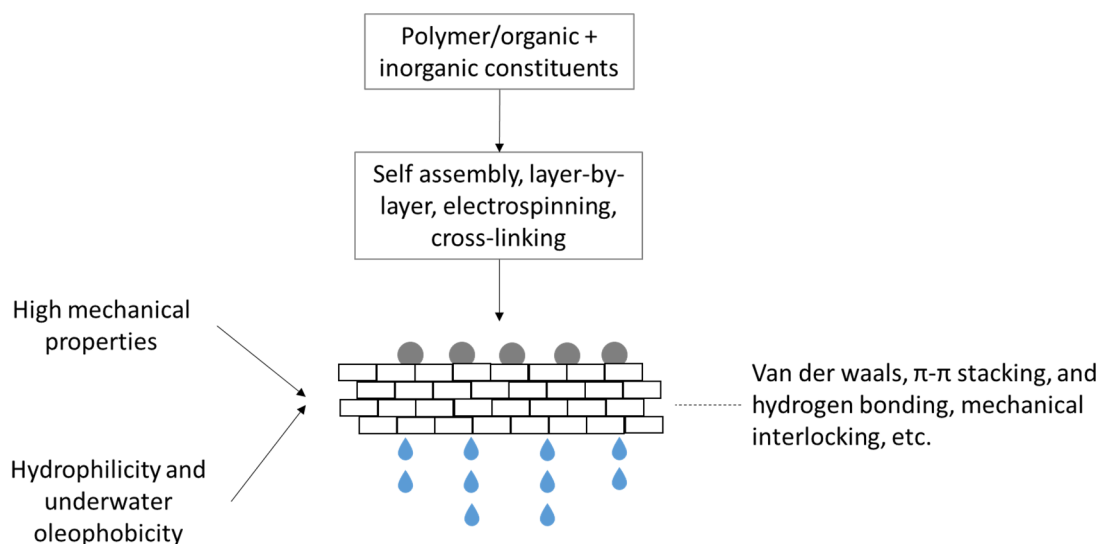


Figure 7. Illustration of the synthesis and interaction of organic and inorganic constituents in layered composites for oil–water separation.

Previous studies have attempted the mass production of artificial nacre by fabricating the following: 3D bulk layered material [46], a millimeter-thick artificial wooden nacre by using a freeze-casting technique that can create a lightweight material [47], large-sized nanocomposite paper through optimization of the interfacial interaction of the lamellar hybrid [107], bulk film through dry-spinning assembly [108], and transparent and tough bulk composite using a vacuum-aided filtration technique [109]. To fabricate large-sized products, the fabrication techniques focus on the alignment of platelets and the creation of mineral bridges, which can be formed due to the diffusion of ions between glass platelets [109]. A similar agreement was shown in a previous study by Jia et al., in which the scale-up of artificial nacre could be performed through a laminating process to regulate interfacial bonding, resulting in a high-performing hierarchical structure [108]. The improvement of mechanical strength through the mineralization of lignocellulose has also been shown in a previous study for the fabrication artificial wooden nacre [47]. Mineralization through the coordination of Ca^{2+} to lignocellulose can close gaps and eliminate flaws within the structure, which can otherwise cause water to reside, resulting in a diminished mechanical strength of the material [47].

6. Conclusions and Outlook

Artificial nacre has been synthesized using various methods with the aim of producing layered composite membranes with high mechanical properties. Among these, self-assembly and layer-by-layer synthesis methods are the most widely used due to the facile fabrication and ease of controlling the membrane's dimension and surface morphology. Vacuum filtration assisted-self-assembly is one of the facile methods used, in which the dimension of membranes can be controlled by varying the volume of solution. However, a large-scale membrane is deemed challenging to be fabricated using this method. Spin coating-assisted layer-by-layer assembly was proven to be able to fabricate various dimensions of membranes, with the ability to control the thickness of each layer with precision. However, this method is quite complex, with many repetitive steps that need to be performed. The treatment of oily wastewater is one of the emerging applications

for artificial nacre, which can effectively treat oil spills. The layered membrane or mussel-inspired composite constituents comply with properties needed to separate the oil–water mixture, especially for superhydrophilicity and underwater oleophobicity. The coating present on natural nacre is applied to artificial membranes such as nacre to enable important self-cleaning properties, in addition to the hydration layer for catechol/chitosan coating in oil–water separation that can effectively separate oil without oil fouling occurring.

The composite membrane shows satisfactory performance in repelling oils, including crude oil, cyclohexane, soybean oil, toluene, silicon oil, engine oil, and so on, with the UOCA value usually being more than 160°. The durability of membranes in seawater environments gives promising results to treat the oil spills. So far, the published studies reveal the potential of artificial nacre to separate oil and water in a lab-scale set-up. However, testing the material for real oily wastewater in a pilot plant has yet to be observed, and this can be an interesting topic to be explored for future studies. Additionally, the enhancement of physical and chemical interactions, such as cross-linking, hydrogen bonding, π – π stacking, etc., among constituents that build the artificial nacre will be an exciting topic to explore due to their contribution to a higher mechanical strength.

Author Contributions: Conceptualization, A.C.K., N.S.S. and H.W.; Writing—original draft preparation, A.C.K., N.S.S., H.W. and Y.F.B.; Writing—review and editing, N.S.S., H.W., Y.F.B., F.A.R., N.J., N.A.K. and H.S.; Supervision, A.C.K., N.S.S. and H.W.; Validation, H.W. All authors have read and agreed to the published version of the manuscript.

Funding: This research and APC were funded by Hibah Publikasi Terindeks Internasional (PUTI): NKB-678/UN2.RST/HKP.05.00/2022 and Universiti Teknologi MARA: 600-RMC/GPK 5/3 (118/2020).

Institutional Review Board Statement: Not applicable.

Informed Consent Statement: Not applicable.

Data Availability Statement: Not applicable.

Conflicts of Interest: The authors declare no conflict of interest.

References

1. Adetunji, A.I.; Olaniran, A.O. Treatment of industrial oily wastewater by advanced technologies: A review. *Appl. Water Sci.* **2021**, *11*, 98. [[CrossRef](#)]
2. Niu, A.; Sun, X.; Lin, C. Trend in Research on Characterization, Environmental Impacts and Treatment of Oily Sludge: A Systematic Review. *Molecules* **2022**, *22*, 7795. [[CrossRef](#)] [[PubMed](#)]
3. Tian, Y.; Zhou, J.; He, C.; He, L.; Li, X.; Sui, H. The Formation, Stabilization and Separation of Oil–Water Emulsions: A Review. *Processes* **2022**, *10*, 738.
4. Samuel, O.; Othman, M.H.D.; Kamaludin, R.; Sinsamphanh, O.; Abdullah, H.; Puteh, M.H.; Kurniawan, T.A.; Li, T.; Ismail, A.F.; Rahman, M.A.; et al. Oilfield-produced water treatment using conventional and membrane-based technologies for beneficial reuse: A critical review. *J. Environ. Manag.* **2022**, *308*, 114556. [[CrossRef](#)]
5. Zolghadr, E.; Firouzjaei, M.D.; Amouzandeh, G.; LeClair, P.; Elliott, M. The Role of Membrane-Based Technologies in Environmental Treatment and Reuse of Produced Water. *Front. Environ. Sci.* **2021**, *9*, 71. [[CrossRef](#)]
6. Medeiros, A.D.; Silva Junior, C.J.; Amorim, J.D.; Durval, I.J.; Costa, A.F.; Sarubbo, L.A. Oily Wastewater Treatment: Methods, Challenges, and Trends. *Processes* **2022**, *10*, 743. [[CrossRef](#)]
7. Abuhasel, K.; Kchaou, M.; Alquraish, M.; Manusamy, Y.; Yong, T.J. Oily Wastewater Treatment: Overview of Conventional and Modern Methods, Challenges, and Future Opportunities. *Water* **2021**, *13*, 980. [[CrossRef](#)]
8. Faisal, W.; Hameed, B.; Almomani, F.; Abdullah, A. A Review on the Treatment of Petroleum Refinery Wastewater Using Advanced Oxidation Processes. *Catalysts* **2021**, *11*, 782. [[CrossRef](#)]
9. Hizam, S.; Bilad, M.; Nordin, N.; Shamsuddin, N. Forward Osmosis for Produced Water Treatment: A Comprehensive Review. *J. Penelit. Dan Pengkaj. Ilmu Pendidik. E-St.* **2021**, *5*, 253–272. [[CrossRef](#)]
10. Han, M.; Zhang, J.; Chu, W.; Chen, J.; Zhou, G. Research Progress and Prospects of Marine Oily Wastewater Treatment: A Review. *Water* **2019**, *11*, 2517. [[CrossRef](#)]
11. Shabani, S.; Khorshidi, B.; Sadrzadeh, M. Chapter 9—Development of nanocomposite membranes by biomimicking nanomaterials. In *Nanocomposite Membranes for Water and Gas Separation*; Sadrzadeh, M., Mohammadi, T., Eds.; Elsevier: Amsterdam, The Netherlands, 2020; pp. 219–236. [[CrossRef](#)]
12. Brock, L.; Sheng, J. Robust Fabrication of Polymeric Nanowire with Anodic Aluminum Oxide Templates. *Micromachines* **2019**, *11*, 46. [[CrossRef](#)] [[PubMed](#)]

13. Wan, C.; Ma, Y.; Gorb, S.N. Compromise between mechanical and chemical protection mechanisms in the *Mytilus edulis* shell. *J. Exp. Biol.* **2019**, *222*, jeb201103. [[CrossRef](#)] [[PubMed](#)]
14. Peng, X.; Zhang, B.; Wang, Z.; Su, W.; Niu, S.; Han, Z.; Ren, L. Bioinspired Strategies for Excellent Mechanical Properties of Composites. *J. Bionic Eng.* **2022**, *19*, 1203–1228. [[CrossRef](#)]
15. Grossman, M.; Bouville, F.; Masania, K.; Studart, A.R. Quantifying the role of mineral bridges on the fracture resistance of nacre-like composites. *Proc. Natl. Acad. Sci. USA* **2018**, *115*, 12698–12703. [[CrossRef](#)]
16. Qiu, T.; Liang, L.; Hao, Y. Thickness effect on the mechanical properties of nacre in *Hyriopsis cumingii* under three-point bending. *Eng. Fract. Mech.* **2022**, *276*, 108869. [[CrossRef](#)]
17. Li, Y.-Y.; Liang, S.-M.; Ji, H.-M.; Li, X.-W. Distinctive Impact of Heat Treatment on the Mechanical Behavior of Nacreous and Crossed-Lamellar Structures in Biological Shells: Critical Role of Organic Matrix. *ACS Biomater. Sci. Eng.* **2022**, *8*, 1143–1155. [[CrossRef](#)] [[PubMed](#)]
18. Jia, Z.; Yu, Y.; Wang, L. Learning from nature: Use material architecture to break the performance tradeoffs. *Mater. Des.* **2019**, *168*, 107650. [[CrossRef](#)]
19. Wang, J.; Cheng, Q.; Tang, Z. Layered nanocomposites inspired by the structure and mechanical properties of nacre. *Chem. Soc. Rev.* **2012**, *41*, 1111–1129. [[CrossRef](#)]
20. Wan, M.-c.; Qin, W.; Lei, C.; Li, Q.-h.; Meng, M.; Fang, M.; Song, W.; Chen, J.-h.; Tay, F.; Niu, L.-n. Biomaterials from the sea: Future building blocks for biomedical applications. *Bioact. Mater.* **2021**, *6*, 4255–4285. [[CrossRef](#)]
21. Porter, M.; McKittrick, J. It's tough to be strong: Advances in bioinspired structural ceramicbased materials. *Am. Ceram. Soc. Bull.* **2014**, *95*, 18–24.
22. Zhang, Y.R.; Du, W.; Zhou, X.D.; Yu, H.Y. Review of research on the mechanical properties of the human tooth. *Int. J. Oral Sci.* **2014**, *6*, 61–69. [[CrossRef](#)] [[PubMed](#)]
23. Liang, B.; Shu, Y.; Wan, P.; Zhao, H.; Dong, S.; Hao, W.; Yin, P. Genipin-enhanced nacre-inspired montmorillonite-chitosan film with superior mechanical and UV-blocking properties. *Compos. Sci. Technol.* **2019**, *182*, 107747. [[CrossRef](#)]
24. Dai, J.; Wang, L.; Wang, Y.; Tian, S.; Tian, X.; Xie, A.; Zhang, R.; Yan, Y.; Pan, J. Robust Nacrelike Graphene Oxide–Calcium Carbonate Hybrid Mesh with Underwater Superoleophobic Property for Highly Efficient Oil/Water Separation. *ACS Appl. Mater. Interfaces* **2020**, *12*, 4482–4493. [[CrossRef](#)]
25. Sun, S.; Mao, L.B.; Lei, Z.; Yu, S.H.; Colfen, H. Hydrogels from Amorphous Calcium Carbonate and Polyacrylic Acid: Bio-Inspired Materials for “Mineral Plastics”. *Angew. Chem. Int. Ed. Engl.* **2016**, *55*, 11765–11769. [[CrossRef](#)] [[PubMed](#)]
26. Shu, Y.; You, T.; Liang, B.; Chen, H.; Yin, P. Bioinspired Ternary Artificial Nacre Graphene Oxide/Carboxyl Functionalized Single-Walled Carbon Nanotubes/Konjac Glucmannan with Enhanced Mechanical Properties. *ACS Appl. Bio Mater.* **2019**, *2*, 5544–5550. [[CrossRef](#)] [[PubMed](#)]
27. Sung, K.; Nakagawa, S.; Kim, C.; Yoshie, N. Fabrication of nacre-like polymer/clay nanocomposites with water-resistant and self-adhesion properties. *J. Colloid Interface Sci.* **2020**, *564*, 113–123. [[CrossRef](#)]
28. Yao, H.-B.; Guan, Y.; Mao, L.-B.; Wang, Y.; Wang, X.-H.; Tao, D.-Q.; Yu, S.-H. A designed multiscale hierarchical assembly process to produce artificial nacre-like freestanding hybrid films with tunable optical properties. *J. Mater. Chem.* **2012**, *22*, 13005–13012. [[CrossRef](#)]
29. Wang, J.; Qiao, J.; Wang, J.; Zhu, Y.; Jiang, L. Bioinspired Hierarchical Alumina-Graphene Oxide-Poly(vinyl alcohol) Artificial Nacre with Optimized Strength and Toughness. *ACS Appl. Mater. Interfaces* **2015**, *7*, 9281–9286. [[CrossRef](#)]
30. Chen, T.; Shi, P.; Zhang, J.; Li, Y.; Tian, X.; Lian, J.; Duan, T.; Zhu, W. Bioinspired enhancement of chitosan nanocomposite films via Mg-ACC crystallization, their robust, hydrophobic and biocompatible. *Appl. Surf. Sci.* **2018**, *459*, 129–137. [[CrossRef](#)]
31. Liang, B.; Zhao, H.; Zhang, Q.; Fan, Y.; Yue, Y.; Yin, P.; Guo, L. Ca²⁺ Enhanced Nacre-Inspired Montmorillonite-Alginate Film with Superior Mechanical, Transparent, Fire Retardancy, and Shape Memory Properties. *ACS Appl. Mater. Interfaces* **2016**, *8*, 28816–28823. [[CrossRef](#)]
32. Wang, Y.; Yuan, H.; Ma, P.; Bai, H.; Chen, M.; Dong, W.; Xie, Y.; Deshmukh, Y.S. Superior Performance of Artificial Nacre Based on Graphene Oxide Nanosheets. *ACS Appl. Mater. Interfaces* **2017**, *9*, 4215–4222. [[CrossRef](#)] [[PubMed](#)]
33. Kuang, Q.; Zhang, D.; Yu, J.C.; Chang, Y.-W.; Yue, M.; Hou, Y.; Yang, M. Toward Record-High Stiffness in Polyurethane Nanocomposites Using Aramid Nanofibers. *J. Phys. Chem. C* **2015**, *119*, 27467–27477. [[CrossRef](#)]
34. Teng, C.; Xie, D.; Wang, J.; Zhu, Y.; Jiang, L. A strong, underwater superoleophobic PNIPAM–clay nanocomposite hydrogel. *J. Mater. Chem. A* **2016**, *4*, 12884–12888. [[CrossRef](#)]
35. Bers, A.V.; D'Souza, F.; Klijnstra, J.W.; Willemsen, P.R.; Wahl, M. Chemical defence in mussels: Antifouling effect of crude extracts of the periostracum of the blue mussel *Mytilus edulis*. *Biofouling* **2006**, *22*, 251–259. [[CrossRef](#)]
36. Obotey Ezugbe, E.; Rathilal, S. Membrane Technologies in Wastewater Treatment: A Review. *Membranes* **2020**, *10*, 89. [[CrossRef](#)] [[PubMed](#)]
37. Verma, D.; Katti, K.S.; Katti, D.R. Effect of biopolymers on structure of hydroxyapatite and interfacial interactions in biomimetically synthesized hydroxyapatite/biopolymer nanocomposites. *Ann. Biomed. Eng.* **2008**, *36*, 1024–1032. [[CrossRef](#)] [[PubMed](#)]
38. Mano, J.A.F. *Biomimetic Approaches for Biomaterials Development*; Wiley-VCH: Hoboken, NJ, USA, 2012.
39. Eckert, A.; Abbasi, M.; Mang, T.; Saalwächter, K.; Walther, A. Structure, Mechanical Properties, and Dynamics of Polyethylenoxide/Nanoclay Nacre-Mimetic Nanocomposites. *Macromolecules* **2020**, *53*, 1716–1725. [[CrossRef](#)]

40. Cheng, M.-m.; Huang, L.-j.; Wang, Y.-x.; Tang, J.-g.; Wang, Y.; Zhao, Y.-c.; Liu, G.-f.; Zhang, Y.; Kipper, M.; Belfiore, L.; et al. Recent developments in graphene-based/nanometal composite filter membranes. *RSC Adv.* **2017**, *7*, 47886–47897. [[CrossRef](#)]
41. Song, P.; Xu, Z.; Wu, Y.; Cheng, Q.; Guo, Q.; Wang, H. Super-tough artificial nacre based on graphene oxide via synergistic interface interactions of π - π stacking and hydrogen bonding. *Carbon* **2017**, *111*, 807–812. [[CrossRef](#)]
42. Kröger, R. Ion binding and nucleation. *Nat. Mater.* **2015**, *14*, 369–370. [[CrossRef](#)] [[PubMed](#)]
43. Zhai, H.; Chu, X.; Li, L.; Xu, X.; Tang, R. Controlled formation of calcium-phosphate-based hybrid mesocrystals by organic–inorganic co-assembly. *Nanoscale* **2010**, *2*, 2456–2462. [[CrossRef](#)] [[PubMed](#)]
44. Tsortos, A.; Nancollas, G.H. The Role of Polycarboxylic Acids in Calcium Phosphate Mineralization. *J. Colloid Interface Sci.* **2002**, *250*, 159–167. [[CrossRef](#)] [[PubMed](#)]
45. Sellinger, A.; Weiss, P.M.; Nguyen, A.; Lu, Y.; Assink, R.A.; Gong, W.; Brinker, C.J. Continuous self-assembly of organic–inorganic nanocomposite coatings that mimic nacre. *Nature* **1998**, *394*, 256–260. [[CrossRef](#)]
46. Gao, H.L.; Chen, S.M.; Mao, L.B.; Song, Z.Q.; Yao, H.B.; Colfen, H.; Luo, X.S.; Zhang, F.; Pan, Z.; Meng, Y.F.; et al. Mass production of bulk artificial nacre with excellent mechanical properties. *Nat. Commun.* **2017**, *8*, 287. [[CrossRef](#)] [[PubMed](#)]
47. Chen, Y.; Fu, J.; Dang, B.; Sun, Q.; Li, H.; Zhai, T. Artificial Wooden Nacre: A High Specific Strength Engineering Material. *ACS Nano*. **2020**, *14*, 2036–2043. [[CrossRef](#)]
48. Mao, L.-b.; Meng, Y.-F.; Meng, X.-S.; Yang, B.; Yang, Y.-L.; Lu, Y.-J.; Yang, Z.-Y.; Shang, L.-M.; Yu, S.-H. Matrix-Directed Mineralization for Bulk Structural Materials. *J. Am. Chem. Soc.* **2022**, *144*, 18175–18194. [[CrossRef](#)]
49. Das, P.; Malho, J.-M.; Rahimi, K.; Schacher, F.H.; Wang, B.; Demco, D.E.; Walther, A. Nacre-mimetics with synthetic nanoclays up to ultrahigh aspect ratios. *Nat. Commun.* **2015**, *6*, 5967. [[CrossRef](#)]
50. Du, G.; Mao, A.; Yu, J.; Hou, J.; Zhao, N.; Han, J.; Zhao, Q.; Gao, W.; Xie, T.; Bai, H. Nacre-mimetic composite with intrinsic self-healing and shape-programming capability. *Nat. Commun.* **2019**, *10*, 800. [[CrossRef](#)]
51. Finnemore, A.; Cunha, P.; Shean, T.; Vignolini, S.; Guldin, S.; Oyen, M.; Steiner, U. Biomimetic layer-by-layer assembly of artificial nacre. *Nat. Commun.* **2012**, *3*, 966. [[CrossRef](#)]
52. Rianasari, I.; Benyettou, F.; Sharma, S.K.; Blanton, T.; Kirmizialtin, S.; Jagannathan, R. A Chemical Template for Synthesis of Molecular Sheets of Calcium Carbonate. *Sci. Rep.* **2016**, *6*, 25393. [[CrossRef](#)]
53. Farhadi-Khouzani, M.; Schütz, C.; Durak, G.M.; Fornell, J.; Sort, J.; Salazar-Alvarez, G.; Bergström, L.; Gebauer, D. A CaCO₃/nanocellulose-based bioinspired nacre-like material. *J. Mater. Chem. A* **2017**, *5*, 16128–16133. [[CrossRef](#)]
54. Shu, Y.; Yin, P.; Liang, B.; Wang, H.; Guo, L. Artificial Nacre-Like Gold Nanoparticles–Layered Double Hydroxide–Poly(vinyl alcohol) Hybrid Film with Multifunctional Properties. *Ind. Eng. Chem. Res.* **2015**, *54*, 8940–8946. [[CrossRef](#)]
55. Wang, J.; Cheng, Q.; Lin, L.; Jiang, L. Synergistic Toughening of Bioinspired Poly(vinyl alcohol) Clay Nanofibrillar Cellulose Artificial Nacre. *ACS Nano*. **2014**, *8*, 2739–2745. [[CrossRef](#)] [[PubMed](#)]
56. Zeng, X.; Ye, L.; Yu, S.; Li, H.; Sun, R.; Xu, J.; Wong, C.P. Artificial nacre-like papers based on noncovalent functionalized boron nitride nanosheets with excellent mechanical and thermally conductive properties. *Nanoscale* **2015**, *7*, 6774–6781. [[CrossRef](#)] [[PubMed](#)]
57. Kou, L.; Gao, C. Bioinspired design and macroscopic assembly of poly(vinyl alcohol)-coated graphene into kilometers-long fibers. *Nanoscale* **2013**, *5*, 4370–4378. [[CrossRef](#)] [[PubMed](#)]
58. Zhu, H.; Cao, H.; Liu, X.; Wang, M.; Meng, X.; Zhou, Q.; Xu, L. Nacre-like composite films with a conductive interconnected network consisting of graphene oxide, polyvinyl alcohol and single-walled carbon nanotubes. *Mater. Des.* **2019**, *175*, 107783. [[CrossRef](#)]
59. Zhang, T.; Sun, J.; Ren, L.; Yao, Y.; Wang, M.; Zeng, X.; Sun, R.; Xu, J.-B.; Wong, C.-P. Nacre-inspired polymer composites with high thermal conductivity and enhanced mechanical strength. *Compos. Part A Appl. Sci. Manuf.* **2019**, *121*, 92–99. [[CrossRef](#)]
60. Wang, P.; Liu, W.; Chen, L.; Mu, C.; Qi, G.; Bian, F. Bio-inspired laminated graphite nanosheets/copper composites. *RSC Adv.* **2015**, *5*, 51342–51346. [[CrossRef](#)]
61. Liu, S.; Ling, J.; Li, K.; Yao, F.; Oderinde, O.; Zhang, Z.; Fu, G. Hierarchical alginate biopolymer papers produced via lanthanide ion coordination. *RSC Adv.* **2016**, *6*, 63171–63177. [[CrossRef](#)]
62. Liu, L.; Gao, Y.; Liu, Q.; Kuang, J.; Zhou, D.; Ju, S.; Han, B.; Zhang, Z. High mechanical performance of layered graphene oxide/poly(vinyl alcohol) nanocomposite films. *Small* **2013**, *9*, 2466–2472. [[CrossRef](#)]
63. Si, L.; Lu, Z.; Yao, C.; Ma, Q.; Zhao, Y.; Wang, Y.; Wang, D.; Jin, Z. Nacre-like nanocomposite film with excellent dielectric insulation properties and mechanical strength based on montmorillonite nanosheet and aramid nanofiber. *J. Mater. Sci.* **2020**, *55*, 5948–5960. [[CrossRef](#)]
64. Wang, Y.; Yu, J.; Chen, L.; Hu, Z.; Shi, Z.; Zhu, J. Nacre-like graphene paper reinforced by polybenzimidazole. *RSC Adv.* **2013**, *3*, 20353–20362. [[CrossRef](#)]
65. Huang, C.; Fang, G.; Deng, Y.; Bhagia, S.; Meng, X.; Tao, Y.; Yong, Q.; Ragauskas, A.J. Robust galactomannan/graphene oxide film with ultra-flexible, gas barrier and self-clean properties. *Compos. Part A Appl. Sci. Manuf.* **2020**, *131*, 105780. [[CrossRef](#)]
66. Yao, Y.; Zeng, X.; Wang, F.; Sun, R.; Xu, J.-b.; Wong, C.-P. Significant Enhancement of Thermal Conductivity in Bioinspired Freestanding Boron Nitride Papers Filled with Graphene Oxide. *Chem. Mater.* **2016**, *28*, 1049–1057. [[CrossRef](#)]
67. Li, Y.; Xue, Z.; Luan, Y.; Wang, L.; Zhao, D.; Xu, F.; Xiao, Y.; Guo, Z.; Wang, Z. Improved mechanical performance of graphene oxide based artificial nacre composites by regulating the micro-laminated structure and interface bonding. *Compos. Sci. Technol.* **2019**, *179*, 63–68. [[CrossRef](#)]

68. Woo, J.Y.; Oh, J.H.; Jo, S.; Han, C.-S. Nacre-Mimetic Graphene Oxide/Cross-Linking Agent Composite Films with Superior Mechanical Properties. *ACS Nano* **2019**, *13*, 4522–4529. [[CrossRef](#)]
69. Wang, Y.; Li, T.; Ma, P.; Zhang, S.; Zhang, H.; Du, M.; Xie, Y.; Chen, M.; Dong, W.; Ming, W. Artificial Nacre from Supramolecular Assembly of Graphene Oxide. *ACS Nano* **2018**, *12*, 6228–6235. [[CrossRef](#)]
70. Yoo, S.C.; Park, Y.K.; Park, C.; Ryu, H.; Hong, S.H. Biomimetic Artificial Nacre: Boron Nitride Nanosheets/Gelatin Nanocomposites for Biomedical Applications. *Adv. Funct. Mater.* **2018**, *28*, 1805948. [[CrossRef](#)]
71. Zhao, N.; Yang, M.; Zhao, Q.; Gao, W.; Xie, T.; Bai, H. Superstretchable Nacre-Mimetic Graphene/Poly(vinyl alcohol) Composite Film Based on Interfacial Architectural Engineering. *ACS Nano* **2017**, *11*, 4777–4784. [[CrossRef](#)]
72. Fang, B.; Peng, L.; Xu, Z.; Gao, C. Wet-Spinning of Continuous Montmorillonite-Graphene Fibers for Fire-Resistant Lightweight Conductors. *ACS Nano* **2015**, *9*, 5214–5222. [[CrossRef](#)]
73. HG, P.K.; Prabhakaran, S.; Xavior, A.; Kalainathan, S.; Lin, D.; Shukla, P.; Vasudevan, V.K. Enhanced surface and mechanical properties of bioinspired nanolaminate graphene-aluminum alloy nanocomposites through laser shock processing for engineering applications. *Mater. Today Commun.* **2018**, *16*, 81–89. [[CrossRef](#)]
74. Han, M.; Shen, W. Nacre-inspired cellulose nanofiber/MXene flexible composite film with mechanical robustness for humidity sensing. *Carbohydr. Polym.* **2022**, *298*, 120109. [[CrossRef](#)] [[PubMed](#)]
75. Yang, W.; Qiu, S.; Zhou, Y.; Zou, B.; Wang, J.; Jia, P.; Song, L. Nanolayered Graphene/Black Phosphorus Films for Fire-Retardant Coatings. *ACS Appl. Nano Mater.* **2022**, *5*, 14841–14849. [[CrossRef](#)]
76. Wang, Q.; Chen, S.; Zeng, S.; Chen, P.; Xu, Y.; Nie, W.; Zhou, Y. Tunable mechanical properties of glass fiber/epoxy composites by incorporating bioinspired montmorillonite-carbon nanotube/epoxy interface layer around the fiber. *Compos. Part B Eng.* **2022**, *242*, 110092. [[CrossRef](#)]
77. Theisen, B.F. Shell cleaning and deposit feeding in *Mytilus edulis* L. (Bivalvia). *Ophelia* **1972**, *10*, 49–55. [[CrossRef](#)]
78. Xu, M.; Sun, T.; Tang, X.; Lu, K.; Jiang, Y.; Cao, S.; Wang, Y. Title: CO₂ and HCl-induced seawater acidification impair the ingestion and digestion of blue mussel *Mytilus edulis*. *Chemosphere* **2020**, *240*, 124821. [[CrossRef](#)]
79. Langton, R.W. Digestive rhythms in the mussel *Mytilus edulis*. *Mar. Biol.* **1977**, *41*, 53–58. [[CrossRef](#)]
80. McHenry, J.G.; Allen, J.A.; Birkbeck, T.H. Effect of tidal submersion on lysozyme activity in *Mytilus edulis* and *Tellina tenuis*. *Mar. Biol.* **1983**, *75*, 57–61. [[CrossRef](#)]
81. Nady, N.; Franssen, M.C.R.; Zuilhof, H.; Eldin, M.S.M.; Boom, R.; Schroën, K. Modification methods for poly(arylsulfone) membranes: A mini-review focusing on surface modification. *Desalination* **2011**, *275*, 1–9. [[CrossRef](#)]
82. Schmidt, M.; Breite, D.; Thomas, I.; Went, M.; Prager, A.; Schulze, A. Polymer membranes for active degradation of complex fouling mixtures. *J. Membr. Sci.* **2018**, *563*, 481–491. [[CrossRef](#)]
83. Wong, P.C.Y.; Lee, J.Y.; Teo, C.W. Application of dispersed and immobilized hydrolases for membrane fouling mitigation in anaerobic membrane bioreactors. *J. Membr. Sci.* **2015**, *491*, 99–109. [[CrossRef](#)]
84. Kolesnyk, I.; Konovalova, V.; Kharchenko, K.; Burban, A.; Knozowska, K.; Kujawski, W.; Kujawa, J. Improved antifouling properties of polyethersulfone membranes modified with α -amylase entrapped in Tetronic® micelles. *J. Membr. Sci.* **2019**, *570–571*, 436–444. [[CrossRef](#)]
85. Mehrabi, Z.; Taheri-Kafrani, A.; Asadnia, M.; Razmjou, A. Bienzymatic modification of polymeric membranes to mitigate biofouling. *Sep. Purif. Technol.* **2020**, *237*, 116464. [[CrossRef](#)]
86. Cloete, W.; Hayward, S.; Swart, P.; Klumperman, B. Degradation of Proteins and Starch by Combined Immobilization of Protease, α -Amylase and β -Galactosidase on a Single Electrospun Nanofibrous Membrane. *Molecules* **2019**, *24*, 508. [[CrossRef](#)] [[PubMed](#)]
87. Kolesnyk, I.; Konovalova, V.; Kharchenko, K.; Burban, A.; Kujawa, J.; Kujawski, W. Enhanced transport and antifouling properties of polyethersulfone membranes modified with α -amylase incorporated in chitosan-based polymeric micelles. *J. Membr. Sci.* **2020**, *595*, 117605. [[CrossRef](#)]
88. Zhao, S.; Tao, Z.; Chen, L.; Han, M.; Zhao, B.; Tian, X.; Wang, L.; Meng, F. An antifouling catechol/chitosan-modified polyvinylidene fluoride membrane for sustainable oil-in-water emulsions separation. *Front. Environ. Sci. Eng.* **2020**, *15*, 63. [[CrossRef](#)]
89. Wang, J.; Wang, H. Multilayered chitosan/kaolin@calcium carbonate composite films with excellent chemical and thermal stabilities for oil/water filtration realized by a facile layer-by-layer assembly. *Sep. Purif. Technol.* **2022**, *289*, 120738. [[CrossRef](#)]
90. Ding, J.; Wang, J.; Luo, X.; Xu, D.; Liu, Y.; Li, P.; Li, S.; Wu, R.; Gao, X.; Liang, H. A passive-active combined strategy for ultrafiltration membrane fouling control in continuous oily wastewater purification. *Water Res.* **2022**, *226*, 119219. [[CrossRef](#)]
91. Gupta, R.K.; Dunderdale, G.J.; England, M.W.; Hozumi, A. Oil/water separation techniques: A review of recent progresses and future directions. *J. Mater. Chem. A* **2017**, *5*, 16025–16058. [[CrossRef](#)]
92. Ahmad, N.A.; Goh, P.S.; Abdul Karim, Z.; Ismail, A.F. Thin Film Composite Membrane for Oily Waste Water Treatment: Recent Advances and Challenges. *Membranes* **2018**, *8*, 86. [[CrossRef](#)]
93. Guo, T.; Heng, L.; Wang, M.; Wang, J.; Jiang, L. Robust Underwater Oil-Repellent Material Inspired by Columnar Nacre. *Adv. Mater.* **2016**, *28*, 8505–8510. [[CrossRef](#)] [[PubMed](#)]
94. Li, B.; Li, L.; Wu, L.; Zhang, J.; Wang, A. Durable Superhydrophobic/Superoleophilic Polyurethane Sponges Inspired by Mussel and Lotus Leaf for the Selective Removal of Organic Pollutants from Water. *ChemPlusChem* **2014**, *79*, 850–856. [[CrossRef](#)]
95. Cao, Y.; Zhang, X.; Tao, L.; Li, K.; Xue, Z.; Feng, L.; Wei, Y. Mussel-Inspired Chemistry and Michael Addition Reaction for Efficient Oil/Water Separation. *ACS Appl. Mater. Interfaces* **2013**, *5*, 4438–4442. [[CrossRef](#)]

96. Li, M.; Chen, Y.; Mao, L.-B.; Jiang, Y.; Liu, M.-F.; Huang, Q.; Yu, Z.; Wang, S.; Yu, S.-H.; Lin, C.; et al. Seeded Mineralization Leads to Hierarchical CaCO₃ Thin Coatings on Fibers for Oil/Water Separation Applications. *Langmuir* **2018**, *34*, 2942–2951. [[CrossRef](#)]
97. Wang, H.; Hu, X.; Ke, Z.; Du, C.Z.; Zheng, L.; Wang, C.; Yuan, Z. Review: Porous Metal Filters and Membranes for Oil-Water Separation. *Nano. Res. Lett.* **2018**, *13*, 284. [[CrossRef](#)]
98. Xu, L.-P.; Peng, J.; Liu, Y.; Wen, Y.; Zhang, X.; Jiang, L.; Wang, S. Nacre-Inspired Design of Mechanical Stable Coating with Underwater Superoleophobicity. *ACS Nano*. **2013**, *7*, 5077–5083. [[CrossRef](#)] [[PubMed](#)]
99. Dong, Y.; Li, J.; Shi, L.; Wang, X.; Guo, Z.; Liu, W. Underwater superoleophobic graphene oxide coated meshes for the separation of oil and water. *Chem. Commun.* **2014**, *50*, 5586–5589. [[CrossRef](#)]
100. Wang, L.; Wang, Y.; Dai, J.; Tian, S.; Xie, A.; Dai, X.; Pan, J. Coordination-driven interfacial cross-linked graphene oxide-alginate nacre mesh with underwater superoleophobicity for oil-water separation. *Carbohydr. Polym.* **2021**, *251*, 117097. [[CrossRef](#)] [[PubMed](#)]
101. Li, J.; Cao, J.; Wei, Z.; Yang, M.; Yin, W.; Yu, K.; Yao, Y.; Lv, H.; He, X.; Leng, J. Electrospun silica/naion hybrid products: Mechanical property improvement, wettability tuning and periodic structure adjustment. *J. Mater. Chem. A* **2014**, *2*, 16569–16576. [[CrossRef](#)]
102. Meng, X.; Wang, M.; Heng, L.; Jiang, L. Underwater Mechanically Robust Oil-Repellent Materials: Combining Conflicting Properties Using a Heterostructure. *Adv. Mater.* **2018**, *30*, 1706634. [[CrossRef](#)]
103. Liu, Y.; Su, Y.; Cao, J.; Guan, J.; Xu, L.; Zhang, R.; He, M.; Zhang, Q.; Fan, L.; Jiang, Z. Synergy of the mechanical, antifouling and permeation properties of a carbon nanotube nanohybrid membrane for efficient oil/water separation. *Nanoscale* **2017**, *9*, 7508–7518. [[CrossRef](#)]
104. Wang, J.; Wang, H. Tolerant chitosan/carboxymethyl cellulose@calcium composite films on nylon fabric for high-flux water/oil separation. *Carbohydr. Polym.* **2022**, *294*, 119832. [[CrossRef](#)] [[PubMed](#)]
105. Harito, C.; Bavykin, D.V.; Yulianto, B.; Dipojono, H.K.; Walsh, F.C. Polymer nanocomposites having a high filler content: Synthesis, structures, properties, and applications. *Nanoscale* **2019**, *11*, 4653–4682. [[CrossRef](#)]
106. George, J.; Ishida, H. A review on the very high nanofiller-content nanocomposites: Their preparation methods and properties with high aspect ratio fillers. *Prog. Polym. Sci.* **2018**, *86*, 1–39. [[CrossRef](#)]
107. Mei, Y.; Tang, X.; Guo, J.; Sun, T.-Y.; Zhang, Y.; Chen, K. Directed Assembly of Large-Sized, Mechanically Robust, Nacre-Inspired Graphene Oxide/Sodium Alginate Nanocomposite Paper. *Macromol. Mater. Eng.* **2020**, *305*, 2000493. [[CrossRef](#)]
108. Jia, H.; Li, Y.; Luan, Y.; Zheng, Y.; Yang, J.; Wang, L.; Guo, Z.; Wu, X. Bioinspired Nacre-like GO-based bulk with easy scale-up process and outstanding mechanical properties. *Compos. Part A Appl. Sci. Manuf.* **2020**, *132*, 105829. [[CrossRef](#)]
109. Magrini, T.; Bouville, F.; Lauria, A.; Le Ferrand, H.; Niebel, T.P.; Studart, A.R. Transparent and tough bulk composites inspired by nacre. *Nat. Commun.* **2019**, *10*, 2794. [[CrossRef](#)] [[PubMed](#)]

Disclaimer/Publisher's Note: The statements, opinions and data contained in all publications are solely those of the individual author(s) and contributor(s) and not of MDPI and/or the editor(s). MDPI and/or the editor(s) disclaim responsibility for any injury to people or property resulting from any ideas, methods, instructions or products referred to in the content.